THE JOURNAL OF BIOLOGICAL CHEMISTRY VOL. 291, NO. 1, pp. 478–492, January 1, 2016

Dynamin-related Protein 1 Oligomerization in Solution Impairs Functional Interactions with Membrane-anchored Mitochondrial Fission Factor*

Received for publication, July 20, 2015, and in revised form, November 4, 2015 Published, JBC Papers in Press, November 17, 2015, DOI 10.1074/jbc.M115.680025

Ryan W. Clinton[‡§¶], **Christopher A. Francy**[‡§¶], **Rajesh Ramachandran**[¶‖], **Xin Qi**[§‖], **and Jason A. Mears**[‡§¶1]

From the [‡]*Department of Pharmacology, the* [§]*Center for Mitochondrial Diseases, the* [¶]*Cleveland Center for Membrane and Structural Biology, and the* [‖]*Department of Physiology and Biophysics, Case Western Reserve University School of Medicine, Cleveland, Ohio 44106*

Mitochondrial fission is a crucial cellular process mediated by the mechanoenzymatic GTPase, dynamin-related protein 1 (Drp1). During mitochondrial division, Drp1 is recruited from the cytosol to the outer mitochondrial membrane by one, or several, integral membrane proteins. One such Drp1 partner protein, mitochondrial fission factor (Mff), is essential for mitochondrial division, but its mechanism of action remains unexplored. Previous studies have been limited by a weak interaction between Drp1 and Mff *in vitro*. Through refined *in vitro* reconstitution approaches and multiple independent assays, we show that removal of the regulatory variable domain (VD) in Drp1 enhances formation of a functional Drp1-Mff copolymer. This protein assembly exhibits greatly stimulated cooperative GTPase activity in solution. Moreover, when Mff was anchored to a lipid template, to mimic a more physiologic environment, significant stimulation of GTPase activity was observed with both WT and ΔVD Drp1. Contrary to recent findings, we show that premature Drp1 self-assembly in solution impairs functional interactions with membrane-anchored Mff. Instead, dimeric Drp1 species are selectively recruited by Mff to initiate assembly of a functional fission complex. Correspondingly, we also found that the coiled-coil motif in Mff is not essential for Drp1 interactions, but rather serves to augment cooperative self-assembly of Drp1 proximal to the membrane. Taken together, our findings provide a mechanism wherein the multimeric states of both Mff and Drp1 regulate their collaborative interaction.

Mitochondria undergo continuous cycles of fission and fusion to maintain a functional organelle network within eukaryotic cells. This mitochondrial network is crucial for ATP generation, apoptotic signaling, and calcium homeostasis. When the proper balance of mitochondrial dynamics is disrupted, mitochondrial dysfunction is observed (1, 2). This insult is associated with increased cell death in several human diseases, including neurodegenerative disorders (3, 4), ischemia-reperfusion injury (5, 6), and glaucoma (7). Therefore, mitochondrial division has developed into a compelling therapeutic target for intervention with small molecule and peptide inhibitors that limit cell death in several of these pathologies (8–13).

The master regulator of mitochondrial fission, dynamin-related protein 1 (Drp1),[2] has been targeted in these diseases. Similar to other dynamin family members, Drp1 is a large GTPase that mediates membrane remodeling. The primary sequence of Drp1 is composed of four conserved regions (see Fig. 1*A*): the GTPase domain, middle domain, variable domain (VD), and GTPase effector domain (GED). Hydrolysis of GTP triggers conformational changes in Drp1 oligomers that generate the mechanical force needed to promote mitochondrial membrane scission (14, 15), and factors that inhibit Drp1 GTPase activity prevent mitochondrial division (8, 16, 17). The middle and GED domains promote Drp1 self-assembly, which is also critical for its role in facilitating mitochondrial fission (18, 19). *In vitro*, the addition of negatively charged lipids increases Drp1 self-assembly to form larger helical assemblies that represent the contractile apparatus of mitochondrial fission (20), and these functional polymers exhibit stimulated GTPase activity (14, 21–23). The VD has recently been shown to act as a negative regulator of Drp1 self-assembly (14) with an inherent ability to interact with cardiolipin (CL) present in mitochondrial membranes (21, 23–25). Studies in yeast have shown that the VD is required for interactions with a mitochondrial adaptor protein (26), but the partner protein identified in that study is not conserved in higher eukaryotes, which suggests that the role of the VD may have evolved in higher organisms to accommodate different regulatory interactions in the cytosol and at the surface of mitochondria.

Drp1 interactions with multiple outer mitochondrial membrane (OMM)-anchored transmembrane proteins have been

* This work was supported by American Heart Association Grants SDG12SDG9130039 (to J. A. M.) and 13BGIA14810010 (to R. R.) and National Institutes of Health Training Grant 2T32GM008803-11A1 (to C. A. F.). This work was also supported by National Institutes of Health Grant R01 NS088192 (to X. Q.). The authors declare that they have no conflicts of interest with the contents of this article. The content is solely the responsibility of the author and does not necessarily represent the official views of the National Institutes of Health.

[1] To whom correspondence should be addressed: 10900 Euclid Ave., Cleveland, OH 44106-4965. Tel.: 216-368-3348; E-mail: jason.mears@case.edu.

[2] The abbreviations used are: Drp1, dynamin-related protein 1 (Drp1); Mff, mitochondrial fission factor; OMM, outer mitochondrial membrane; VD, variable domain; GED, GTPase effector domain; CC, coiled-coil; TM, transmembrane; BME, β-mercaptoethanol; DOPC, 1,2-dioleoyl-*sn*-glycero-3-phosphocholine; DGS-NTA(Ni^{2+}), 3.3% 1,2-dioleoyl-*sn*-glycero-3-[(*N*-(5-amino-1-carboxypentyl)iminodiacetic acid)succinyl] (nickel salt); IMAC, immobilized metal affinity chromatography; IEX, ion exchange; SEC, size exclusion chromatography; MALS, multi-angle light scattering; PE, phosphatidylethanolamine; SL, scaffold liposomes; CL, cardiolipin; MEF, mouse embryonic fibroblast.

identified to promote its recruitment to the mitochondria (26–28). One such protein is mitochondrial fission factor (Mff), and genetic studies have unambiguously shown that Mff is critical for Drp1 recruitment to the OMM. In fact, Mff deletion suppresses Drp1 localization to mitochondria (29), which results in an excessively interconnected mitochondrial network (30). Concomitantly, overexpression of Mff results in excessive mitochondrial fission (29). Although Drp1-Mff interactions are crucial for mitochondrial dynamics, the interaction between Drp1 and Mff appears to be transient. Previous studies report that Drp1 GTPase activity is either unaffected (31) or mildly enhanced *in vitro* in the presence of Mff (32). Additionally, crosslinking agents are required to capture a stable complex using pulldown experiments (29, 30). Given this relatively weak affinity, the molecular basis for Drp1-Mff interactions remains uncharacterized.

Using a combination of biochemical, cellular, and EM methods, we have examined the structural and functional ramifications of Drp1 and Mff interactions *in vitro*. The role of the VD in Mff interactions was investigated by examining established assembly mutants and distinct Drp1 isoforms. We find that the Drp1 VD negatively regulates the assembly of a functional fission complex dependent on Drp1 interaction with Mff. Using mutations that alter the oligomeric state of Drp1 in solution, we show that Mff selectively assembles Drp1 dimers into large complexes with greatly stimulated GTPase activity. Our results also show that the conserved coiled-coil (CC) motif in Mff improves the efficiency of Drp1 recruitment and provides a scaffold to coordinate Drp1 assembly. Therefore, effective, functional interactions within the mitochondrial fission complex are shaped by the oligomeric tendencies of both Drp1 and Mff.

Experimental Procedures

Protein Constructs and Mutagenesis—Drp1 Isoforms 1 and 3 (Drp1-1 and Drp1-3; UniProt IDs O00429-1 and O00429-4) and Drp1 Isoform 1 lacking residues 517–639 (ΔVD) were cloned into a pCal-n-EK vector with a human rhinovirus 3C protease (HR3CP) site as described previously (14). Mff lacking its transmembrane (TM) segment (MffΔTM; UniProt ID Q9GZY8-5, residues 1–218) and Mff lacking both its CC and its TM (Mff ΔCC-TM; residues 1–186) were cloned into pET28a with a C-terminal His_6 affinity tag using NcoI and HindIII restriction sites introduced during PCR amplification. Site-directed mutagenesis was performed using the QuikChange Lightning kit (Agilent).

Protein Expression and Purification—All Drp1 constructs were expressed in BL21-(DE3) Star *Escherichia coli* in LB broth for 24 h at 18 °C after induction with 1 mM isopropyl-1-thio-β-D-galactopyranoside. Cells were harvested by centrifugation, and then stored at −60 °C until purification. Cells were resuspended in Cal-A buffer (0.5 M L-arginine, pH 7.5, 0.3 M NaCl, 5 mM $MgCl_2$, 2 mM $CaCl_2$, 1 mM imidazole, and 10 mM BME) with Pefabloc-SC (0.5 mM final), and cells were lysed by sonication on ice. Cell lysates were cleared by centrifugation at 150,000 × *g* for 1 h at 4 °C, and the supernatant was isolated. Affinity capture was performed using gravity filtration with calmodulin agarose (Agilent) pre-equilibrated with fresh Cal-A buffer. After the supernatant was loaded, the resin was washed with 25 column volumes of Cal-A followed by 8 elutions with 0.5 column volumes of Cal-B buffer (0.5 M L-arginine, pH 7.5, 0.3 M NaCl, 2.5 mM EGTA, and 10 mM BME). Protein-containing fractions were pooled and incubated overnight at 4 °C with His-tagged HR3CP. This solution was concentrated using a 30,000 molecular weight cut-off centrifugal concentrator for all constructs excluding ΔVD due to its propensity to polymerize and fall out of solution. Protein samples were further purified by size exclusion chromatography (SEC) using an ÄKTA Purifier FPLC (GE Healthcare) and a Superdex 200 16/600 column equilibrated with a HEPES column buffer containing 150 mM salt (HCB150: 50 mM HEPES(KOH), pH 7.5, 0.15 M KCl, and 10 mM BME) and 5 mM $MgCl_2$. All Drp1-containing fractions resolved by the column were collected and concentrated, and glycerol was added to 5% final. This isolated protein was aliquoted, frozen, and stored at −60 °C until use.

Mff was expressed in BL21-(DE3) *E. coli* in LB broth for 4 h at 30 °C after induction with 0.5 mM isopropyl-1-thio-β-D-galactopyranoside. Cells were harvested by centrifugation and stored at −60 °C until purification. Cells were resuspended in immobilized metal affinity chromatography (IMAC)-A buffer (50 mM Tris-HCl, pH 7.5, 0.5 M NaCl, 20 mM imidazole, 10 mM BME) with Pefabloc-SC (0.5 mM final), and cells were lysed by sonication on ice. Cell lysates were cleared as described above, and affinity capture was performed using FPLC and a prepacked HiTrap IMAC column (GE Healthcare) charged with Ni^{2+} and equilibrated with IMAC-B (50 mM Tris-HCl, pH 7.5, 0.1 M NaCl, 20 mM imidazole, 10 mM BME). Clarified lysate was loaded onto the column, and then washed to baseline with IMAC-B. Mff was eluted from the column with a linear gradient from 0 to 100% IMAC-C (50 mM Tris-HCl, pH 7.5, 0.1 M NaCl, 250 mM imidazole, 10 mM BME) over 10 column volumes. Protein-containing fractions were pooled, diluted 10-fold in ion exchange (IEX)-A (50 mM Tris-HCl, pH 7.5, 10 mM BME), and loaded onto a Q Sepharose anion exchange column (GE Healthcare). The column was washed to baseline with IEX-A, and Mff was eluted by the addition of 10% IEX-B (50 mM Tris-HCl, pH 7.5, 1 M NaCl, 10 mM BME). Peak Mff fractions were pooled, concentrated, and subjected to SEC using a Superdex 200 16/600 column with HEPES column buffer containing 300 mM salt (HCB300: 50 mM HEPES (KOH), pH 7.5; 0.3 M NaCl; 10 mM BME). Mff peak fractions were pooled and concentrated with a 10,000 molecular weight cut-off centrifugal concentrator, 5% glycerol was added, and aliquots were frozen and stored at −60 °C until use.

Liposome Preparation—Three distinct lipid formulations were utilized in this study: scaffold liposomes (SL: 96.7% 1,2-dioleoyl-*sn*-glycero-3-phosphocholine (DOPC), 3.3% 1,2-dioleoyl-*sn*-glycero-3-[(*N*-(5-amino-1-carboxypentyl)iminodiacetic acid)succinyl] (nickel salt) (DGS-NTA(Ni^{2+}))); scaffold liposomes with cardiolipin (SL/CL: 86.8% DOPC, 3.3% DGS-NTA(Ni^{2+}), 9.9% bovine heart cardiolipin); and scaffold liposomes with phosphatidylethanolamine (PE) and CL (SL/PE/CL: 51.8% DOPC, 3.3% DGS-NTA(Ni^{2+}), 35% 1,2-dioleoyl-*sn*-glycero-3-phosphoethanolamine (DOPE), and 9.9% bovine heart cardiolipin). All lipids used in this study were purchased from Avanti Polar Lipids (Alabaster, AL). Lipids were mixed

and dried to a thin film with a stream of nitrogen gas. Trace solvent was removed with a SpeedVac at 37 °C for 1 h immediately after films were prepared. The lipids were rehydrated in HCB150 for 30 min in a 37 °C water bath with occasional vortexing. Resuspended lipid solutions were freeze-thawed and extruded through a 1.0-μm polycarbonate filter. Lipid solutions were stored at 4 °C or on ice until use.

GTPase Assay—Drp1 GTPase activity was determined using a colorimetric phosphate generation assay (33) with some modifications. Briefly, Mff (4.95 μM final) was diluted to 4× with HCB150 in the presence or absence of SL or SL/CL (150 μM total lipid final) for 15 min at room temperature. This solution was added to 1.2× Drp1 (500 nM final), and then incubated for an additional 15 min at room temperature. 3× GTP/Mg^{2+} (1 mM and 2 mM final, respectively) in HCB150 was added to Drp1/Mff mixtures to start reactions, and samples were incubated at 37 °C. At the designated time points, EDTA (0.1 M final) was added to sample aliquots. Malachite green reagent (1 mM malachite green carbinol, 10 mM ammonium molybdate tetrahydrate, and 1 N HCl) was added to each sample, and OD_{650} was measured using a VersaMax microplate reader (Molecular Devices). Using Excel (Microsoft), the obtained raw phosphate levels were converted into rates using all data that contributed to a linear trend (minimum of three time points). These rates were converted to k_{cat} by accounting for Drp1 concentration and plotted in GraphPad Prism 6. Statistical significance was determined using an unpaired *t* test.

The concentration dependence of Mff-induced stimulation of Drp1 GTPase activity was assayed using varying Mff concentrations. The obtained k_{cat} was plotted as a function of Mff concentration, and the data were fit with the nonlinear log(agonist) *versus* response fit using GraphPad Prism 6.

Negative Stain Transmission Electron Microscopy—For all microscopy, samples were prepared as indicated, adsorbed to carbon-coated grids, and stained with 2% uranyl acetate. Samples were visualized on a Tecnai T12 (FEI Co.) electron microscope at 100 keV, and images were acquired using a Gatan 4k × 4k camera at a magnification of 49,000× (in the absence of liposomes) or 18,500× (in the presence of liposomes).

Size Exclusion Chromatography with Multi-angle Light Scattering—To accurately determine the oligomeric distribution of Drp1 in solution, proteins were fractionated on a Superose 6 10/300 GL SEC column in HCB150 containing 1 mM DTT rather than BME. Column eluate was analyzed by tandem miniDAWN TREOS MALS and Optilab rEX differential refractive index detectors (Wyatt Technologies) as described previously (23). Molar mass was determined using the ASTRA 6.1 software package (Wyatt technologies) and was plotted with molar mass (right axes) and normalized refractive index (left axes) as a function of elution volume. Drp1-3 (10 μM), ΔVD (6 μM), and Mff (75 μM) and corresponding mutants were loaded in a total volume of 0.5 ml.

Co-sedimentation Assay—To identify proteins within oligomeric complexes, an ultracentrifugation sedimentation assay was used. Briefly, Drp1 constructs (2 μM) in the absence and presence of MffΔTM (10 μM) were combined in HCB150 for 2 h at room temperature. Samples were centrifuged 30 min at 160,000 × *g* at 4 °C. Supernatant was discarded, and pellets were washed and recentrifuged twice. The final pellet was resuspended in 1× Laemmli buffer, resolved by SDS-PAGE, and stained with Instant Blue (Expedeon, Cambridge UK) to identify proteins that sedimented in oligomeric complexes.

Glutaraldehyde Crosslinking EMSA—Mff interactions with ΔVD and ΔVD^{G363D} were investigated using a chemical crosslinking electrophoretic mobility shift assay. Briefly, 3 μM ΔVD or ΔVD^{G363D} was incubated for 30 min in the presence or absence of 15 μM MffΔTM in HCB150. Each protein combination was treated with either HCB150 or 5.5 mM glutaraldehyde diluted in HCB150 for 30 min at room temperature. Crosslinking was quenched with Tris-HCl, pH 7.5, at a final concentration of 150 mM for at least 15 min at room temperature. Samples were dissolved in Laemmli buffer and resolved by SDS-PAGE. Completed SDS-PAGE gels were either stained for total protein by Instant Blue (Expedeon) or transferred to a PVDF membrane, and Mff was detected using an anti-His antibody (1:3,000, Thermo Scientific).

Cell Culture and Immunocytochemistry—All mouse embryonic fibroblasts (MEFs) were maintained in DMEM supplemented with 10% heat-inactivated FBS and 1% penicillin/streptomycin at 37 °C in 5% CO_2/95% air. Cells were transfected with 1 μg of plasmid DNA encoding Myc-tagged Drp1 Isoform 1, Myc-Drp1 Isoform 3, or Myc-Drp1 ΔVD using *Trans*IT-2020 transfection reagent (Mirus Bio, Madison, WI) according to the manufacturer's protocol.

Cells cultured on coverslips were washed with cold PBS, fixed in 4% formaldehyde, and permeabilized with 0.1% Triton X-100. After incubation with 2% normal goat serum (to block nonspecific staining), fixed cells were incubated overnight at 4 °C with rabbit anti-Tom20 (1:500; Santa Cruz Biotechnology, Santa Cruz, CA) and mouse anti-Myc (1:500; Santa Cruz Biotechnology) primary antibodies. Cells were washed with PBS and incubated with Alexa Fluor 488-conjugated anti-mouse and Alexa Fluor 568-conjugated anti-rabbit secondary antibodies (1:500; Invitrogen) for 60 min at room temperature. Coverslips were mounted on glass slides and imaged by confocal fluorescence microscopy using an Olympus FV1000 IX81 confocal microscope (Olympus USA).

To quantitate mitochondrial fragmentation, cells were immunostained with anti-Tom20 and anti-Myc antibodies as described. Mitochondrial morphology was then examined in Myc-Drp1-expressing cells. The percentage of Myc-Drp1-expressing cells with fragmented mitochondria relative to the total number of Myc-Drp1-expressing cells was calculated. To quantitate Drp1 localization on the mitochondria, Pearson's co-efficient of ΔVD localization on mitochondria was calculated in cells expressing Drp1 ΔVD.

Assessment of Drp1 Expression in MEFs—Drp1 KO MEFs were transfected with the indicated plasmids as described. Total protein was harvested 24 h after transfection, and protein concentration was determined by Bradford assay. Thirty μg of total protein was resuspended in Laemmli buffer, resolved by SDS-PAGE, and transferred onto nitrocellulose membranes. Membranes were probed with anti-Myc and anti-actin antibodies (1:1000 dilution for both, Sigma-Aldrich) followed by visualization using enhanced chemiluminescence.

Results

The Variable Domain of Drp1 Limits Productive Interaction with Mff—In this study, Drp1 constructs were expressed and isolated as described previously (14), and the affinity tag was removed to examine the properties of the native Drp1 sequence. Initially, the role of the VD was investigated given its proposed role in interactions with partner proteins (26). To study this region, the previously characterized VD deletion mutant (ΔVD) was expressed and isolated (14, 22). Recent studies have implied that different Drp1 isoforms may have distinct cellular interactions (34), but the functional role of these sequence changes is not fully understood. Therefore, Drp1 splice variants with maximal (Isoform 1, or Drp1-1) and minimal (Isoform 3, or Drp1-3) sequence inclusion in the VD were also used to examine Drp1-Mff interactions (Figs. 1 and 2). The basal GTPase activity of each construct was assessed using a colorimetric assay, as described previously (33), and the k_{cat} of both Drp1-1 and Drp1-3 was found to be 1.8 min^{-1} (Fig. 1*B*), which is consistent with previous studies using tagless or His-tagged Drp1 constructs (21, 23). The GTPase activity of ΔVD was slightly diminished when compared with WT constructs (0.98 min^{-1}), which was also observed previously (14, 22).

To characterize the interaction between Mff and Drp1, the GTPase activities of Drp1-1, Drp1-3, and ΔVD were measured in the absence and presence of MffΔTM-His_6 (referred to as Mff from here on). Consistent with previous studies (31), no difference in the GTPase activity of Drp1-1 and Drp1-3 was observed when Mff was present in solution. However, the GTPase activity of ΔVD was stimulated more than 10-fold when Mff was present (Fig. 1*B*). This stimulation of ΔVD by Mff was dependent on concentration (Fig. 1*C*), and Mff at 5 μM was shown to elicit the maximal response. Therefore, this concentration of Mff was used in all subsequent GTPase assays.

To further examine interactions between Drp1 and Mff, negative stain EM analysis was used to assess the formation of distinct macromolecular complexes. Samples were made that contained Drp1 alone and, separately, Drp1 was incubated with a 5-fold molar excess of the cytosolic portion of Mff lacking its TM segment (MffΔTM; residues 1–218). When each of the Drp1 constructs were examined alone, small protein complexes were readily observed (Fig. 1, *E–G*), and no large polymers were apparent. In the case of Drp1-1 and Drp1-3, these complexes likely represent smaller multimeric Drp1 species that predominate at this concentration (Fig. 1*D*) (23).

When Mff was added to the Drp1-1 and Drp1-3 solutions, the protein complexes appeared to be small and well dispersed (Fig. 1, *H–I*), and larger complexes were still absent. Conversely, when Mff was added to ΔVD in solution (Fig. 1*J*), large filamentous polymers were observed with an average diameter of 24.2 ± 2.6 nm (n = 384). This increased assembly of Drp1 into filaments was consistent with the observed stimulation in GTPase activity (Fig. 1*B*). Therefore, we demonstrate that removal of the VD favors Drp1-Mff interactions, which parallels recent findings (35). In addition, we now show that this interaction nucleates the formation of large, functional protein complexes.

As the VD has been shown to regulate Drp1 self-assembly (14), we examined the oligomeric propensities of WT and ΔVD Drp1 using size exclusion chromatography coupled to multi-angle light scattering (SEC-MALS) analyses (Fig. 1*D*). Consistent with previous studies (23), Drp1-3 was shown to equilibrate between dimers and higher-order multimers (Fig. 1*D*, *black*), and a similar trend was observed for Drp1-1 (see the accompanying article (42)). Conversely, ΔVD was found to be exclusively dimeric (Fig. 1*D*, *red*). The role of the VD in regulating Drp1 self-assembly was previously demonstrated as assembly-primed, calmodulin-binding peptide (CBP)-tagged ΔVD efficiently formed oligomers in solution and bound to lipid (14). However, at the concentrations used in these studies with untagged protein, assembly-competent ΔVD dimers formed large polymers only in the presence of Mff. Collectively, these results show that Mff preferentially supports stable assembly of Drp1ΔVD dimers in solution.

Tethering of Mff to Liposome Scaffolds Stimulates Drp1-3 and ΔVD GTPase Activity—Although robust oligomerization and stimulation of ΔVD GTPase activity were observed in the presence of Mff, no corresponding changes were observed with Drp1-1 and Drp1-3 in solution. Because Mff is an integral membrane protein, a model system was developed to mimic Drp1-Mff interactions proximal to a lipid bilayer.

A His_6 tag engineered at the C terminus of Mff was used as a handle to tether the protein on SL containing 3.3 mol % DGS-NTA(Ni^{2+}) lipid (Fig. 2*A*). In this way, Mff is oriented at the lipid bilayer with its C terminus anchored to the membrane surface akin to the native protein. A similar approach has previously been employed to study interactions of other proteins at the plasma membrane (36, 37). Using this strategy, Mff abundance at the membrane surface and the stoichiometry of Mff-Drp1 interactions could be tightly controlled. Moreover, the lipid composition used was intentionally inert (96.7% DOPC) to exclusively measure the effect of tethered Mff on Drp1 function, and not Drp1 stimulation by lipid alone. A separate lipid mixture that incorporated 10 mol % CL, termed scaffold lipid with cardiolipin (SL/CL), was used to explore the potential role of this dimeric, negatively charged phospholipid in promoting interactions between Drp1 and Mff. Importantly, this lower CL concentration also limits lipid stimulation of Drp1 GTPase activity and ensures that any changes in enzyme activity were principally due to interactions with Mff on the lipid template. Consistent with earlier studies (23), we found that GTPase activity of Drp1 was not significantly altered in the presence of either lipid mixture (≤20% difference in activity when SL or SL/CL was added).

When these topology-enforced liposomes were used, stimulation of WT Drp1 GTPase activity was observed in the presence of Mff. However, under these conditions, this change was dependent on the Drp1 isoform used. For Drp1-1, GTPase activity was unaffected by the addition of Mff tethered to either SL or SL/CL (Fig. 2, *B* and *C*). On the other hand, Drp1-3 exhibited a 1.8-fold stimulation (3.2 min^{-1}) in the presence of Mff-decorated SL (Fig. 2*B*). The presence of CL in the lipid template significantly enhanced the stimulation in activity (2.6-fold increase) when Drp1-3 was added to SL/CL with Mff (5.1 min^{-1}, $p < 0.0005$; Fig. 2*C*).

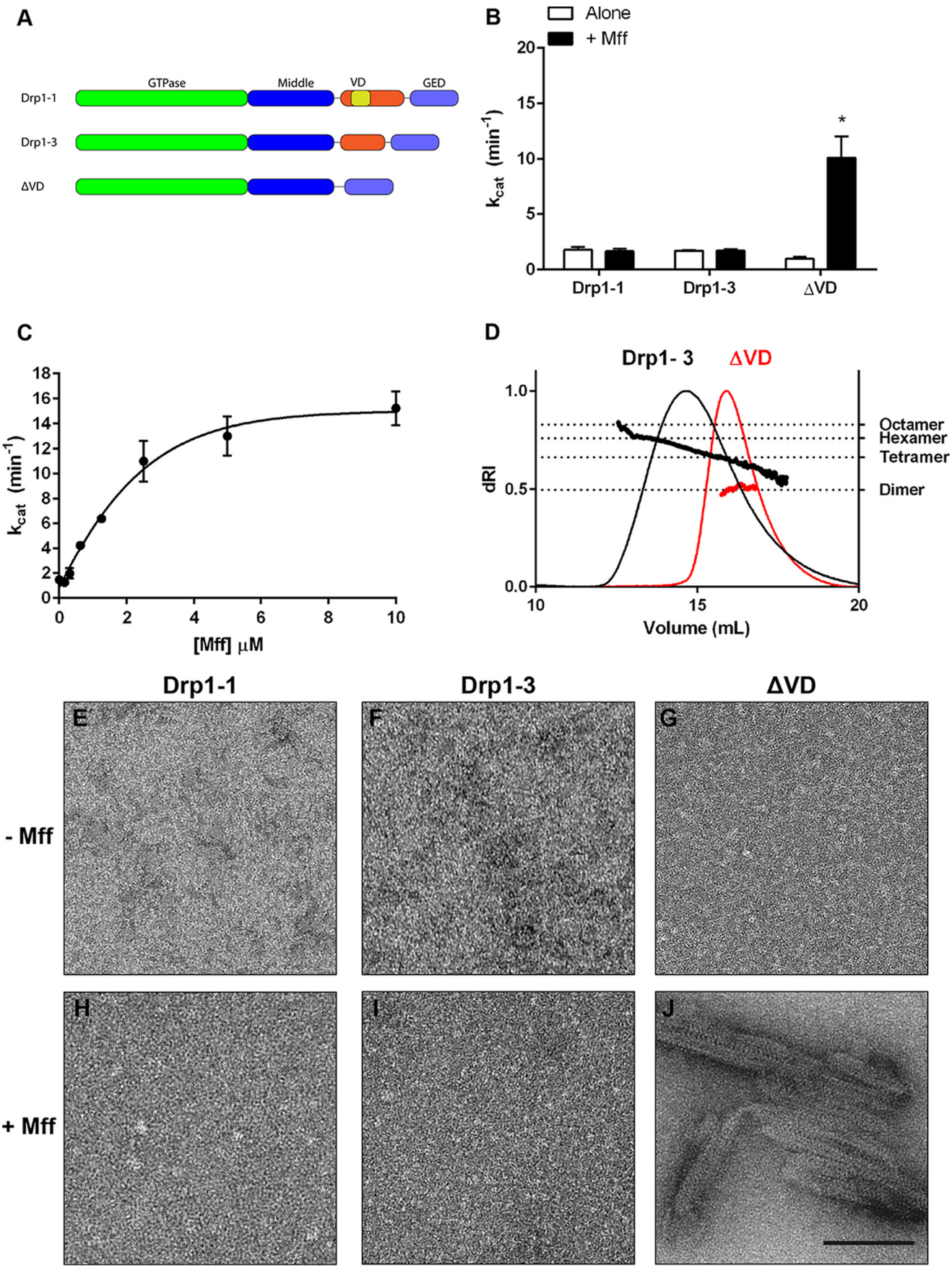
A
GTPase
Middle
VD
GED
Drp1-1
Drp1-3
ΔVD
B
Alone
+ Mff
k_{cat} (min^{-1})
20
15
10
5
0
*
Drp1-1
Drp1-3
ΔVD
C
k_{cat} (min^{-1})
18
16
14
12
10
8
6
4
2
0
0
2
4
6
8
10
[Mff] μM
D
Drp1- 3
ΔVD
dRI
1.0
0.5
0.0
Octamer
Hexamer
Tetramer
Dimer
10
15
20
Volume (mL)
Drp1-1
Drp1-3
ΔVD
- Mff
+ Mff
E
F
G
H
I
J

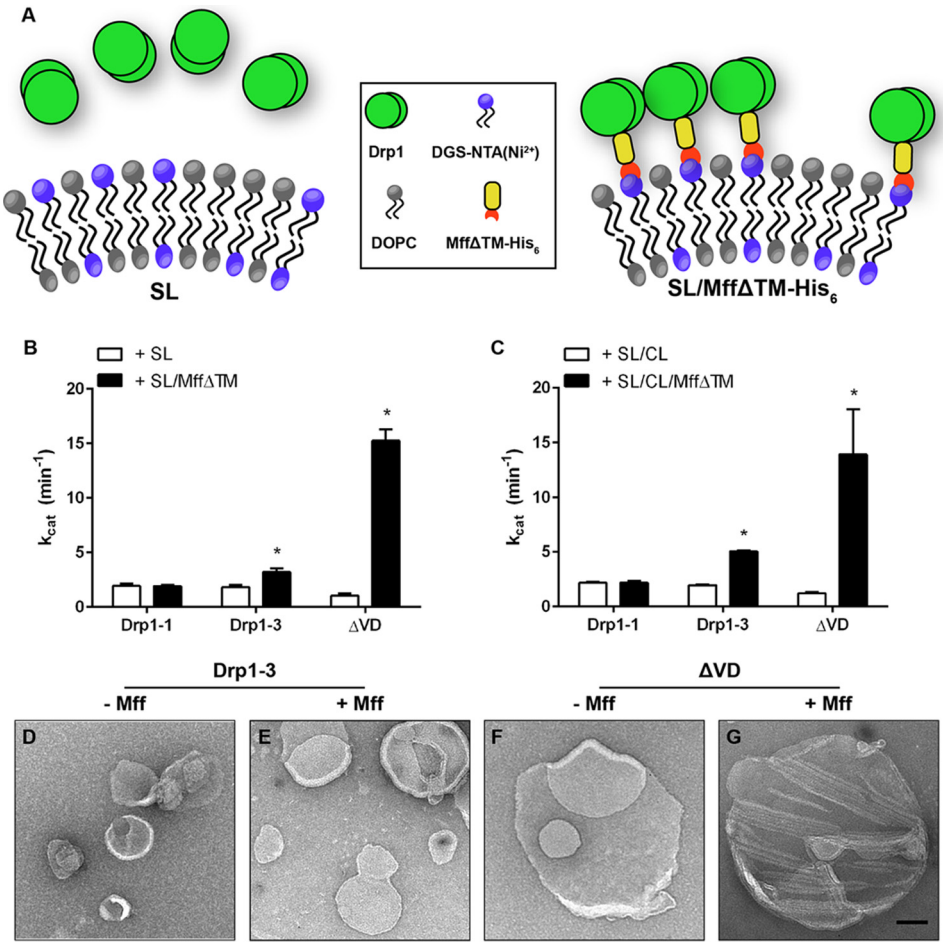

FIGURE 2. **Coupling of Mff to topology-enforcing liposomes enhances Drp1 stimulation.** *A*, schematic representations of the scaffold liposomes used in this study. Drp1 does not interact with liposomes in the absence of Mff (*left*), but Drp1 is recruited to Mff-decorated liposomes (*right*). *B* and *C*, GTPase activities were measured for Drp1-1, Drp1-3, and ΔVD (0.5 μM for each) in the absence (*white*) or presence (*black*) of Mff (5 μM) tethered to SL (*B*) and SL templates with 10% CL (SL/CL: 150 μM) (*C*). *, $p < 0.0005$. *D–G*, negative stain EM images of Drp1-3 (*D* and *E*) and ΔVD (*F* and G) (1 μM) added to scaffold liposomes (SL: 150 μM) in the absence (*D* and *F*) or presence (*E* and *G*) of MffΔTM (5 μM). *Scale bar*, 100 nm.

When compared with WT Drp1, ΔVD GTPase activity was more robustly stimulated in the presence of Mff-decorated liposomes, which is consistent with experiments performed in solution (Fig. 1*B*). Mff tethering slightly enhanced stimulation of ΔVD activity ($k_{cat} = 15.2$ min^{-1}, an ~15-fold increase when compared with a 10-fold increase in solution; Fig. 2*B*), which reflects the increased local concentration of Mff on the membrane. When ΔVD was added to Mff coupled to SL/CL, a comparable stimulation (13.9 min^{-1}) was observed that was not significantly distinct from the stimulation on SL ($p = 0.46$, Fig. 2*C*). Therefore, the enhanced stimulation observed with Drp1-3 in the presence of limiting amounts of CL was attributed to VD interactions with the lipid template that were otherwise missing in the deletion mutant.

When examined by EM, no discernible remodeling was observed when Drp1-3 or ΔVD was added to lipid templates lacking Mff, and no macromolecular complexes were observed (Fig. 2, *D* and *F*, respectively). This result is consistent with the lack of stimulated GTPase activity. Interestingly, when Drp1-3 was incubated with Mff-decorated liposomes, there was no evident membrane remodeling (Fig. 2*E*), although GTPase activity stimulation was observed (Fig. 2, *B* and *C*). When these templates were pre-incubated with Mff, the addition of ΔVD led to the formation of filamentous protein structures on the surface of the liposomes (Fig. 2*G*), and these structures were similar to those found in solution (Fig. 1*J*). The increase in stimulated GTPase activity, when compared with Drp1-3, is attributed to the greater abundance and enhanced assembly of Drp1 polymers mediated by Mff interactions at the surface of the liposome.

Alterations within the VD Modulate Drp1-mediated Mitochondrial Fission in MEFs—Because there was a clear distinction in the activities of Drp1 splice variants and the ΔVD

FIGURE 1. **The VD of Drp1 is a negative-regulator of Mff-induced self-assembly.** *A*, schematic representation of the proteins used in this study, including WT Drp1 Isoforms 1 and 3 (Drp1-1 and Drp1-3) and the ΔVD mutant. The GTPase, middle, VD, and GED domains are highlighted. The *yellow region* in Drp1-1 represents the alternatively spliced B-insert. *B*, GTPase activity of Drp1-1, Drp1-3, and ΔVD (0.5 μM final for each) in the absence (*white*) or presence (*black*) of Mff (5 μM) in solution. *, $p < 0.0005$. *C*, GTPase activity of ΔVD (0.5 μM final) in the presence of MffΔTM at various concentrations. *D*, SEC-MALS was used to assess the solution oligomer state of Drp1-3 (*black trace*) and ΔVD (*red trace*). *Dotted lines* on the right axis correspond to the indicated oligomer based on the predicted molecular mass of indicated Drp1 multimers. *dRI*, normalized differential refractive index. *E–J*, negative stain EM images of Drp1-1 (*E* and *H*), Drp1-3 (*F* and *I*), and ΔVD (*G* and *J*) are shown in the absence (*E–G*) or presence (*H–J*) of Mff. *Scale bar*, 100 nm.

mutant, each of these proteins was expressed in MEFs lacking Drp1 ($Drp1^{-/-}$ MEFs) (38) and changes in mitochondrial morphology were evaluated. Overexpression of Myc-tagged Drp1-1, Drp1-3, and ΔVD in $Drp1^{-/-}$MEFs (Fig. 3, *A* and *C*) resulted in significant mitochondrial fragmentation (Fig. 3*B*). Overexpression of all Myc-Drp1 constructs was capable of rescuing significant mitochondrial fragmentation within these cells lacking endogenous Drp1, although Drp1-3 overexpression resulted in a more potent effect than did Drp1-1 (Fig. 3*B*). Interestingly, mitochondrial fission was observed when ΔVD was overexpressed, but its effect was significantly diminished when compared with WT proteins (Fig. 3*B*). Thus, the inclusion of the VD results in a more efficient fission machinery in cells, and alternative splicing can modulate this activity.

To examine the recruitment of ΔVD to the OMM in cells, the same construct was expressed in WT and Mff-knock-out (Mff^{WT} and $Mff^{-/-}$ respectively) MEFs (Fig. 3*D*). Little, if any, mitochondrial fragmentation was observed when comparing Mff^{WT} and $Drp1^{-/-}$ MEFs using a control vector (Fig. 3, *B* and *E*). Overexpression of ΔVD led to a significant increase in fragmentation in both cell lines, and this response was greatly attenuated in $Mff^{-/-}$ MEFs (Fig. 3*E*). This reduction in fission was attributed to decreased recruitment of ΔVD in cells lacking Mff, as ΔVD was efficiently recruited to the mitochondria in Mff^{WT} MEFs. This recruitment was reduced by ~50% in $Mff^{-/-}$ MEFs (Fig. 3*F*). Based on these findings, Mff targets ΔVD to mitochondria, but fission appears to be impeded post-recruitment.

The Assembly-incompetent Drp1 G363D Mutant Is Insensitive to Mff Interactions—Drp1-Mff interactions with the greatest stimulation in GTPase activity appeared to be dependent on the ability of Drp1 to self-assemble into higher-order oligomers. In fact, the ΔVD mutant has previously been shown to potentiate Drp1 assembly into larger polymers (14). This could explain the enhanced Mff-induced oligomerization of ΔVD when compared with Drp1-3, as well as the increased stimulation in GTPase activity. To test this idea, the assembly-defective Drp1 G363D mutant was used. This middle domain mutation prevents Drp1 self-assembly into species larger than a dimer (18, 39).

To confirm the oligomeric potency of the G363D mutant ($Drp1\text{-}3^{G363D}$) when compared with WT Drp1, SEC-MALS was used. As shown previously (23), Drp1-3 in solution exists as a mixture of dimers and higher-order multimers (Fig. 4*A*, *black trace*). When the G363D mutation was introduced to the Drp1-3 construct ($Drp1\text{-}3^{G363D}$), the isolated protein migrated predominantly as a dimer in solution (Fig. 4*A*, *blue trace*). In solution, the $Drp1\text{-}3^{G363D}$ mutant did not exhibit any defect in GTPase activity when compared with WT (Fig. 4*C*), and GTPase activity was unaffected when undecorated SL or SL/CL were added (Fig. 5, *A* and *F*). Unlike Drp1-3, the assembly-incompetent $Drp1\text{-}3^{G363D}$ did not exhibit stimulated GTPase activity when it was added to Mff-decorated SL or SL/CL templates (Fig. 5, *A* and *F*, respectively). This result shows that the Mff-induced stimulation of GTPase activity reflects enhanced Drp1 self-assembly proximal to the membrane template.

To complement these studies, a double mutant was generated that combined the G363D and ΔVD mutations (ΔVD^{G363D}). This mutant was designed to restrict the self-assembly properties of ΔVD that result in higher-order oligomers. SEC-MALS analysis revealed that ΔVD^{G363D} is also predominantly dimeric (Fig. 4*B*, *blue trace*). Therefore, ΔVD and ΔVD^{G363D} are both dimers and only differ in their ability to form higher-order oligomers. This mutant allowed us to directly evaluate the role of Drp1 self-assembly on Mff-induced polymerization and GTPase stimulation.

The GTPase activity of ΔVD^{G363D} was similar to ΔVD, and the double mutant did not exhibit an increase in activity when assayed in the presence of undecorated SL or SL/CL (Fig. 5, *B* and *G*). Although the addition of Mff to ΔVD in solution yields an ~10-fold stimulation in activity, no stimulation was observed with ΔVD^{G363D} (Fig. 4*D*). Moreover, stimulation in the presence of Mff coupled to SL or SL/CL was completely abolished when using the ΔVD^{G363D} mutant (Fig. 5, *B* and *G*, respectively). EM analyses confirmed these findings as the large filamentous structures observed when ΔVD was added to Mff (Fig. 4*E*) were not observed using ΔVD^{G363D} (Fig. 4*F*). Similarly, the liposome-targeted filamentous structures observed when ΔVD was added to Mff-decorated SL (Fig. 5*C*) were not detected when ΔVD^{G363D} was incubated with the same template (Fig. 5*D*). Based on these results, Mff stimulates Drp1 activity by supporting cooperative self-assembly into large, filamentous structures.

Although the G363D mutation prevents Drp1 self-assembly, it was unclear whether this dimeric mutant could still interact with Mff. Co-sedimentation analysis showed that ΔVD formed stable complexes with Mff, but consistent with our EM observations, ΔVD^{G363D} was unable to form large polymers that would sediment (Fig. 4*H*). To capture short-lived intermediates of Drp1-Mff in solution, a nonspecific amine-to-amine chemical crosslinker, glutaraldehyde, was utilized. Electrophoretic mobility shifts were visualized by SDS-PAGE and Western blot analyses to identify covalently linked Drp1-Mff complexes. Both ΔVD and ΔVD^{G363D} were found to interact with MffΔTM in solution as unique complexes were observed. We also noticed that MffΔTM was shifted into larger molecular weight complexes, which demonstrates an association with both ΔVD and ΔVD^{G363D} (Fig. 4*I*). Collectively, these experiments demonstrate that Drp1 dimers clearly interact with Mff, but Drp1 self-assembly is required for complex stabilization. Consequently, Mff may act as a scaffold for Drp1 self-assembly, which stimulates GTPase activity.

Higher-order Self-assembly of Drp1 R376E Prohibits Functional Interactions with Mff—Given that Drp1-3 and ΔVD GTPase activities were stimulated by Mff interactions *in vitro*, we sought to characterize the putative Mff binding-defective mutant, Drp1 R376E (40). This charge reversal was designed to disrupt an interaction interface between Drp1 and Mff, and Mff immunoprecipitation of Drp1 from HEK293 cells in the presence of a crosslinker was inhibited (40). The recently solved crystal structure of Drp1 reveals that Arg-376 is situated in close proximity to an assembly interface, interface 4, unique to Drp1 (22). Thus, two alternative explanations for the observed lack of interaction between Mff and the R376E mutant are possible. Namely, destabilization of this novel self-assembly interface could alter the self-assembly properties of Drp1, which in

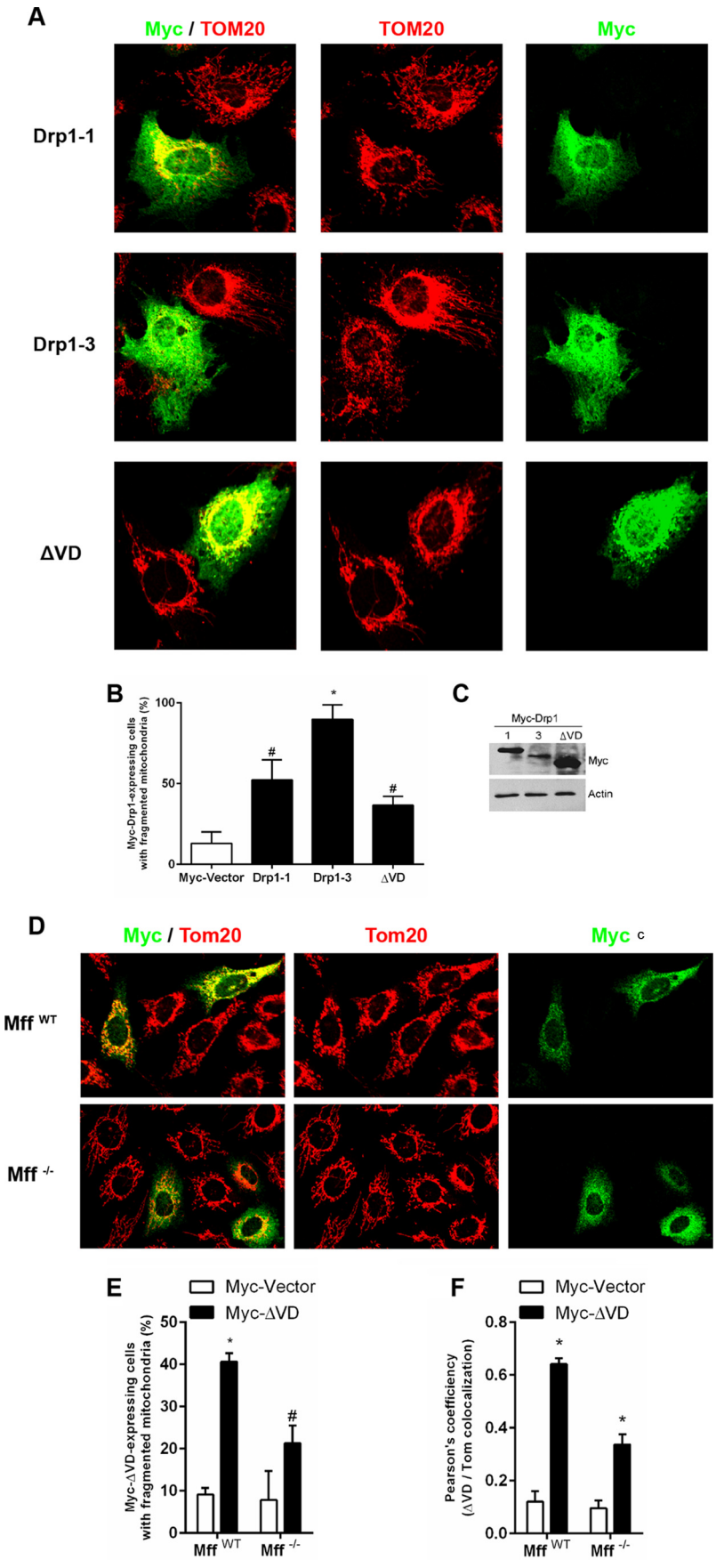
A
Myc / TOM20
TOM20
Myc
Drp1-1
Drp1-3
ΔVD
B
Myc-Drp1-expressing cells with fragmented mitochondria (%)
100
50
0
Myc-Vector
Drp1-1
Drp1-3
ΔVD
C
Myc-Drp1
1
3
ΔVD
Myc
Actin
D
Myc / Tom20
Tom20
Myc
Mff WT
Mff -/-
E
Myc-Vector
Myc-ΔVD
Myc-ΔVD-expressing cells with fragmented mitochondria (%)
50
40
30
20
10
0
Mff WT
Mff -/-
F
Myc-Vector
Myc-ΔVD
Pearson's coefficiency (ΔVD / Tom colocalization)
0.8
0.6
0.4
0.2
0.0
Mff WT
Mff -/-

turn affects Mff interactions. On the other hand, this mutation could result in a direct perturbation of the Mff interaction interface as originally interpreted. To distinguish between these possibilities, the R376E mutation was introduced within the Drp1-3 and ΔVD constructs (termed Drp1-3^{R376E} and ΔVD^{R376E}, respectively) to examine whether this single residue modification could alter Drp1 interactions with Mff.

Following from the observation that the Mff-induced stimulation of Drp1 activity was intimately linked to the oligomeric state of Drp1, SEC-MALS was used to assess the R376E mutation in the contexts of full-length Drp1-3 and ΔVD. When compared with Drp1-3 (Fig. 4*A*, *black trace*) at equivalent concentration, the Drp1-3^{R376E} mutant exhibited a propensity to form higher-order multimers (Fig. 4*A*, *red trace*). In agreement, previous studies assessing the assembly competence of $Drp1^{R376E}$ found that this mutant was enriched in larger complexes (~700 kDa) and depleted in smaller complexes (~160 kDa) in cell lysates (40). Therefore, this mutant provides an opportunity to assess functional Mff interactions with larger Drp1 multimers.

When compared with WT Drp1 (Drp1-3), the R376E mutant exhibited an equivalent basal GTPase activity, and no stimulation was observed when Mff was present in solution (Fig. 4*C*). Unlike Drp1-3, the addition of Mff-tethered liposomes had no stimulatory effect on the activity of the Drp1-3^{R376E} mutant (Fig. 5, *A* and *F*, respectively). EM studies confirmed that although Drp1-3^{R376E} is an assembly-competent mutant (*i.e.* it readily polymerizes in the presence of GTP analogs), it was unable to form large oligomers on Mff-decorated liposomes (not shown). Thus, the prevalence of higher-order Drp1 multimers in solution impairs functional interaction with membrane-anchored Mff.

Having established that Drp1ΔVD exists predominantly as a dimer in solution that polymerizes in the presence of Mff, the impact of the R376E mutation on cooperative ΔVD-Mff assembly was assessed. Remarkably, the R376E mutant remained exclusively dimeric in the absence of the VD (Fig. 4*B*, *red trace*). In striking contrast to the prematurely multimerized Drp1-3^{R376E}, the addition of Mff to ΔVD^{R376E} in solution enhanced GTPase activity ~5-fold (2.8 min^{-1}; Fig. 4*D*). EM analysis of ΔVD^{R376E} in the presence of Mff in solution shows an abundance of filamentous oligomers (Fig. 4*G*) analogous to those formed by ΔVD in the presence of Mff (Fig. 4*E*). This demonstrates that the R376E mutation does not directly disrupt Drp1-Mff interaction. However, the ΔVD^{R376E}-Mff assemblies in solution were not as large or as ordered as those seen with ΔVD and Mff, which agrees with the less prolific stimulation in activity (~5-fold for ΔVD^{R376E} *versus* ~10-fold for ΔVD).

Functional assembly of ΔVD and ΔVD^{R376E} with Mff tethered to either SL or SL/CL was comparable. GTPase activity of ΔVD^{R376E} was stimulated 20- and 16-fold using Mff-decorated SL and SL/CL templates, respectively (k_{cat} = 12.7 min^{-1} for ΔVD^{R376E} with SL + Mff and 13 min^{-1} for ΔVD^{R376E} with SL/CL + Mff; Fig. 5, *B* and *G*). Moreover, the addition of ΔVD^{R376E} to Mff-tethered lipid templates led to formation of filamentous complexes (Fig. 5*E*) that were similar to ΔVD oligomers under the same conditions (Fig. 5*C*). Collectively, these results demonstrate that the R376E mutation does not directly inhibit interactions between Drp1 and Mff. Rather, the Drp1-3^{R376E} mutant augments the propensity of the full-length protein to multimerize in solution, and this equilibrium shift toward higher-order multimers impairs Mff-induced self-assembly on membranes. Removal of the VD reverts the prematurely multimeric full-length Drp1-3^{R376E} to predominantly dimeric species, which rescues functional interactions with Mff.

Mff Multimerization Enhances Drp1 Assembly and GTPase Activity—Having established that the multimeric state of Drp1 potentiates interactions with Mff, we sought to examine whether sequence variation in Mff would affect Mff-induced Drp1 assembly. We focused on two domains conserved among all Mff splice variants: a pair of N-terminal repeats and a conserved CC motif immediately preceding its TM segment (Fig. 6*A*). These domains are particularly interesting because each domain distinctly impacts Mff function. The repeat domains have been shown to be important for interaction with Drp1, whereas the CC has been implicated in Mff multimerization (30–32).

We first mutated the 4-amino acid core of each individual repeat (VPER or VPEK) to alanines, and then found that either mutation resulted in a great reduction of Mff solubility. Due to this reduced solubility, these mutants were deemed unusable. On the other hand, deletion of the CC domain yielded soluble protein, so its role in Drp1-Mff interactions was explored.

SEC-MALS analysis revealed that MffΔTM (26 kDa) is predominantly a tetramer in solution (Fig. 6*B*, *black trace*). By striking contrast, MffΔCC-TM (22 kDa) was exclusively monomeric (Fig. 6*B*, *green trace*), which clearly demonstrates the role of the CC motif in Mff multimerization. Additionally, the MffΔCC-TM mutant was unable to stimulate ΔVD self-assembly or GTPase activity in solution (Fig. 6, *C* and *G*, respectively). Thus, the CC motif plays an important role in Mff tetramerization, which coordinates stable ΔVD interactions to promote assembly of filamentous polymers.

On the other hand, the tethering of MffΔCC-TM to a membrane template improved its ability to stimulate ΔVD activity (Fig. 6*H*). Consistent with this observation, ΔVD polymerization was observed when it was added to liposomes decorated with MffΔCC-TM (Fig. 6*F*). Moreover, membrane deformation was observed leading to the formation of well ordered helical oligomers of ΔVD on the template. Therefore, the high local

FIGURE 3. **The VD is not essential for mitochondrial targeting and subsequent fission in MEF cells.** *A*, representative fluorescence micrographs of $Drp1^{-/-}$ MEFs transfected with Myc-tagged Drp1-1, Drp1-3, or ΔVD. Confocal imaging analysis was carried out using anti-Myc (*green*) and anti-Tom20 (a marker of mitochondria, *red*) antibodies. *B*, mitochondrial fragmentation within transfected cells was quantitated as the percentage of Myc-Drp1-expressing cells with fragmented mitochondria relative to total Myc-expressing cells. *C*, Western blot analysis of Myc-Drp1 expression in Drp1 knock-out MEFs 24 h after transfection. Actin was used as a loading control. *D*, Mff^{WT} (*top*) and $Mff^{-/-}$ (*bottom*) MEFs were transfected with Myc-ΔVD. Confocal imaging analysis was carried out using anti-Myc (*green*) and anti-Tom20 (*red*) antibodies. *E*, quantitation of mitochondrial fragmentation in Mff^{WT} (*white*) and $Mff^{-/-}$ (*black*) MEFs expressing Myc-ΔVD. *F*, ΔVD/Tom20 co-localization in *D* was determined from confocal images by calculating the Pearson's co-efficient. #, $p > 0.05$ and *, $p > 0.0005$ when compared with Myc-vector transfected cells.

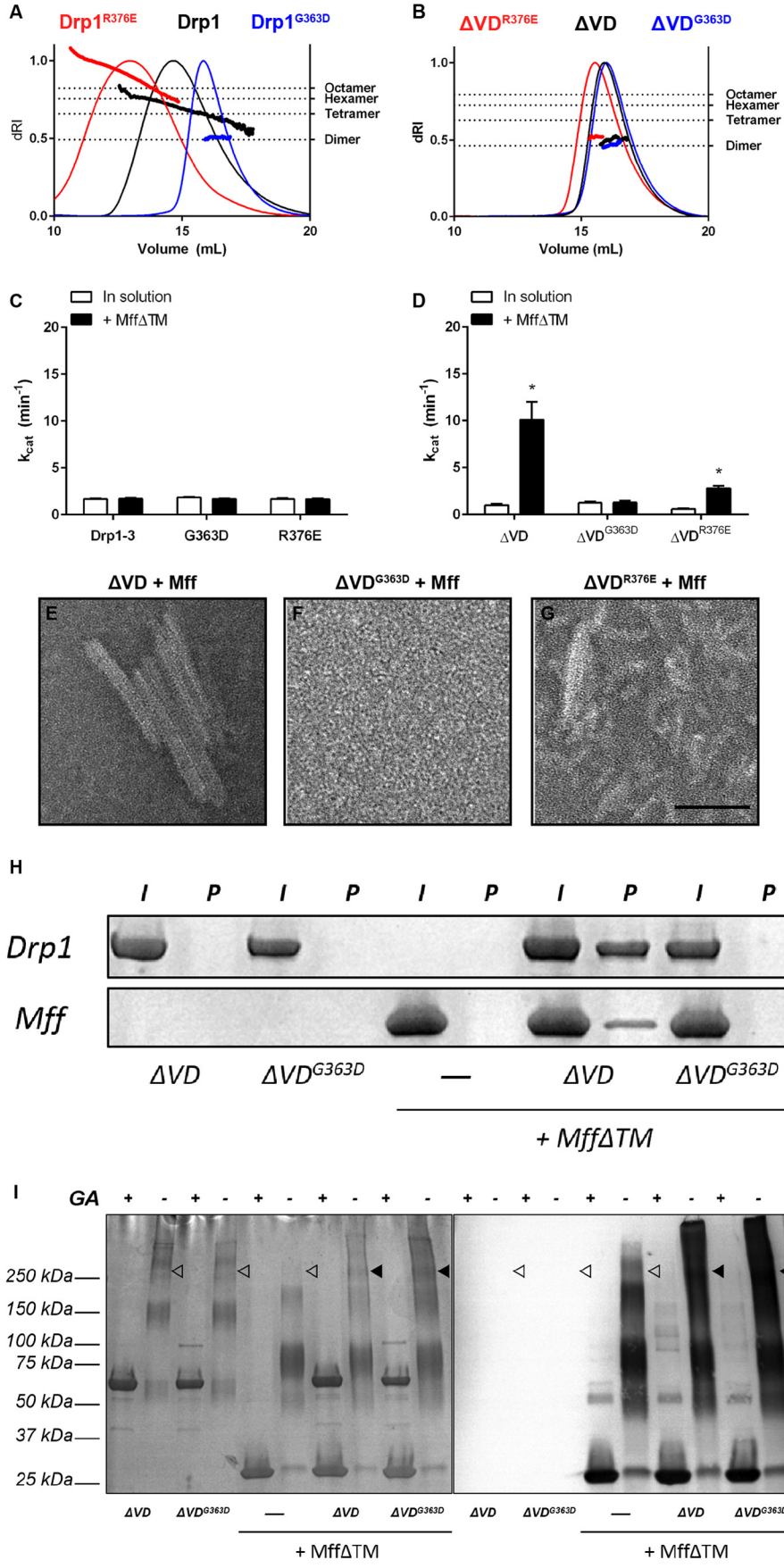
A
Drp1R376E
Drp1
Drp1G363D
dRI
Octamer
Hexamer
Tetramer
Dimer
Volume (mL)
B
ΔVDR376E
ΔVD
ΔVDG363D
C
In solution
+ MffΔTM
kcat (min-1)
Drp1-3
G363D
R376E
D
ΔVD
ΔVDG363D
ΔVDR376E
ΔVD + Mff
ΔVDG363D + Mff
ΔVDR376E + Mff
E
F
G
H
I
Drp1
Mff
GA
250 kDa
150 kDa
100 kDa
75 kDa
50 kDa
37 kDa
25 kDa
+ MffΔTM

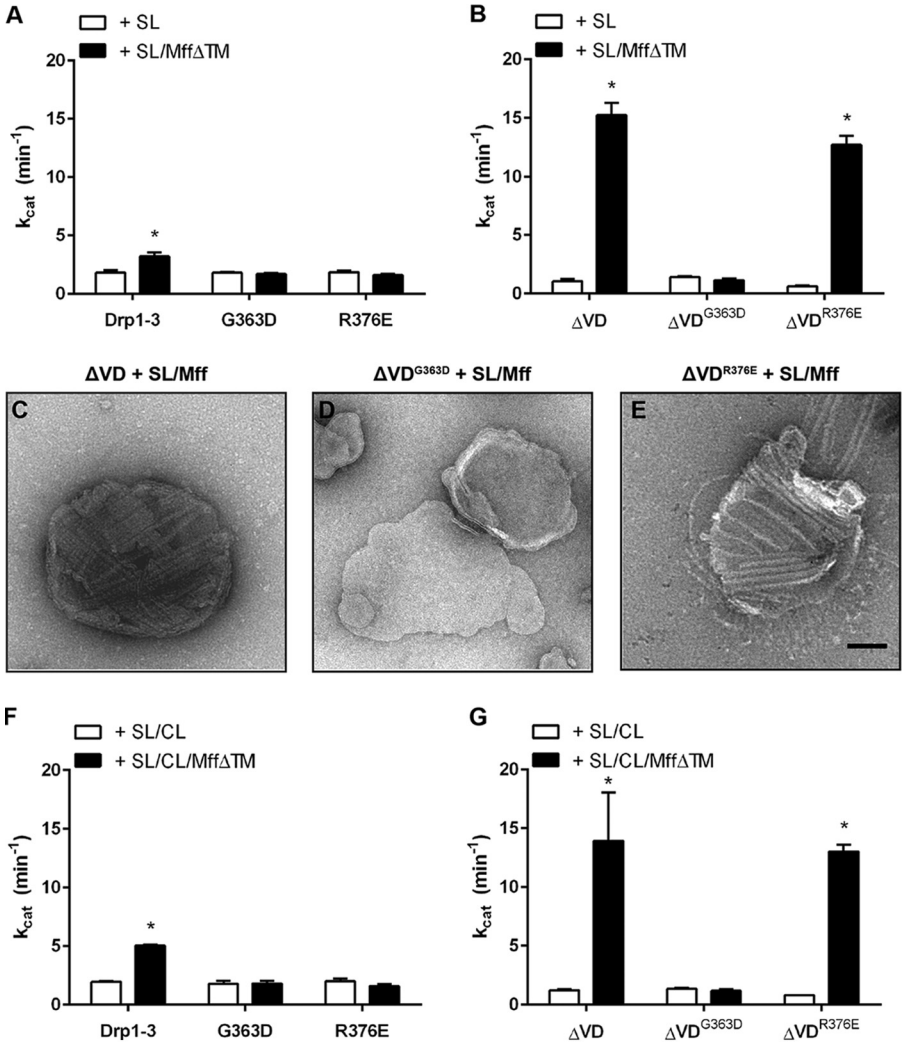

FIGURE 5. **Removal of the VD rescues the R376E defect in Mff-induced assembly.** *A*, GTPase activity of Drp1-3, Drp1-3^{G363D}, and Drp1-3^{R376E} (0.5 μM final) was determined in the presence of undecorated liposomes (*white*, SL: 150 μM final) or Mff-decorated liposomes (*black*, SL/MffΔTM: 150 μM/5 μM final). *B*, GTPase activity of ΔVD, ΔVD^{G363D} and ΔVD^{R376E} (0.5 μM final) was determined in the presence of undecorated liposomes (*white*, SL: 150 μM final) or Mff-decorated liposomes (*black*, SL/MffΔTM: 150 μM/5 μM final). *C–E*, negative stain EM of ΔVD (*C*), ΔVD^{G363D} (*D*), or ΔVD^{R376E} (*E*) (1 μM each) incubated with Mff-decorated liposomes (SL/MffΔTM: 150 μM/5 μM). *Scale bar*, 100 nm. *F*, GTPase activity of Drp1-3, Drp1-3^{G363D}, and Drp1-3^{R376E} (0.5 μM final) in the presence of liposomes with limited CL (*white*, SL/CL: 150 μM final) or the same liposomes decorated with Mff (*black*, SL/CL/MffΔTM: 150 μM/5 μM final). *G*, GTPase activity of ΔVD, ΔVD^{G363D}, and ΔVD^{R376E} (0.5 μM final) in the presence of liposomes with limited CL (*white*, SL/CL: 150 μM final) or the same liposomes decorated with Mff (*black*, SL/CL/MffΔTM: 150 μM/5 μM final). *, $p < 0.0005$.

concentration of MffΔCC-TM on the lipid scaffold enhanced stable interactions with Drp1 to promote oligomerization. This result shows that removal of the CC, and subsequent disruption of the Mff tetramer, allowed the Drp1 oligomers to enforce lipid curvature. Conversely, Mff tetramers, assembled via the CC motif, provided a less flexible scaffold that interacted with Drp1 to nucleate filamentous assemblies on the lipid surface. Based on this observation, we concluded that limited mobility of Mff complexes resists Drp1-induced remodeling of the lipid template.

Because removal of the CC motif from Mff allowed Drp1 to impose curvature on the SL/CL template, a more malleable lipid template was examined with MffΔTM tethered. Previous studies have shown that the addition of PE to liposomes results in a more fluid lipid bilayer that Drp1 can more readily deform (23). Therefore, a third lipid mixture (SL/PE/CL) was generated

FIGURE 4. **Mutations that alter the multimeric equilibrium of Drp1 interfere with Mff-induced self-assembly.** *A* and *B*, SEC-MALS was used to assess the multimeric distributions of WT and mutant proteins. WT Drp1 (Isoform 3, *black trace*) is compared with the G363D (*blue*) and R376E (*red*) mutants in *A*. ΔVD (*black trace*) and the corresponding double mutants ΔVD^{G363D} (*blue*) and ΔVD^{R376E} (*red*) are shown in *B*. *Dotted lines* indicate the predicted molecular masses of Drp1 multimers. *dRI*, normalized differential refractive index. *C*, GTPase activity was measured for Drp1-3, Drp1-3^{G363D}, and Drp1-3^{R376E} in solution in the absence (*white*) and presence (*black*) of Mff. *D*, similarly, GTPase activity was measured for ΔVD, ΔVD^{G363D}, and ΔVD^{R376E} in solution in the absence (*white*) and presence (*black*) of Mff. *, $p < 0.0005$. *E–G*, negative stain EM images of MffΔTM (5 μM) incubated with ΔVD (*E*), ΔVD^{G363D} (*F*), and ΔVD^{R376E} (*G*). *Scale bar*, 100 nm. *H*, MffΔTM (10 μM) was co-sedimented with Drp1-1, ΔVD, and ΔVD^{G363D} (2 μM each) using ultracentrifugation. The input (*I*) and the final washed pellet (*P*) were separated by SDS-PAGE and stained with Instant Blue. *I*, MffΔTM (15 μM) was incubated alone, or with ΔVD and ΔVD^{G363D} (3 μM each) in the presence or absence of glutaraldehyde (*GA*) for 30 min. Samples were resolved by SDS-PAGE, and then stained with Instant Blue (*left*). Mff was detected using an anti-His_6 antibody (*right*). A high molecular mass band was observed in samples containing Mff crosslinked with ΔVD and ΔVD^{G363D} (indicated by *filled arrowheads*). The same complex is not observed in other samples (indicated by *open arrowheads*).

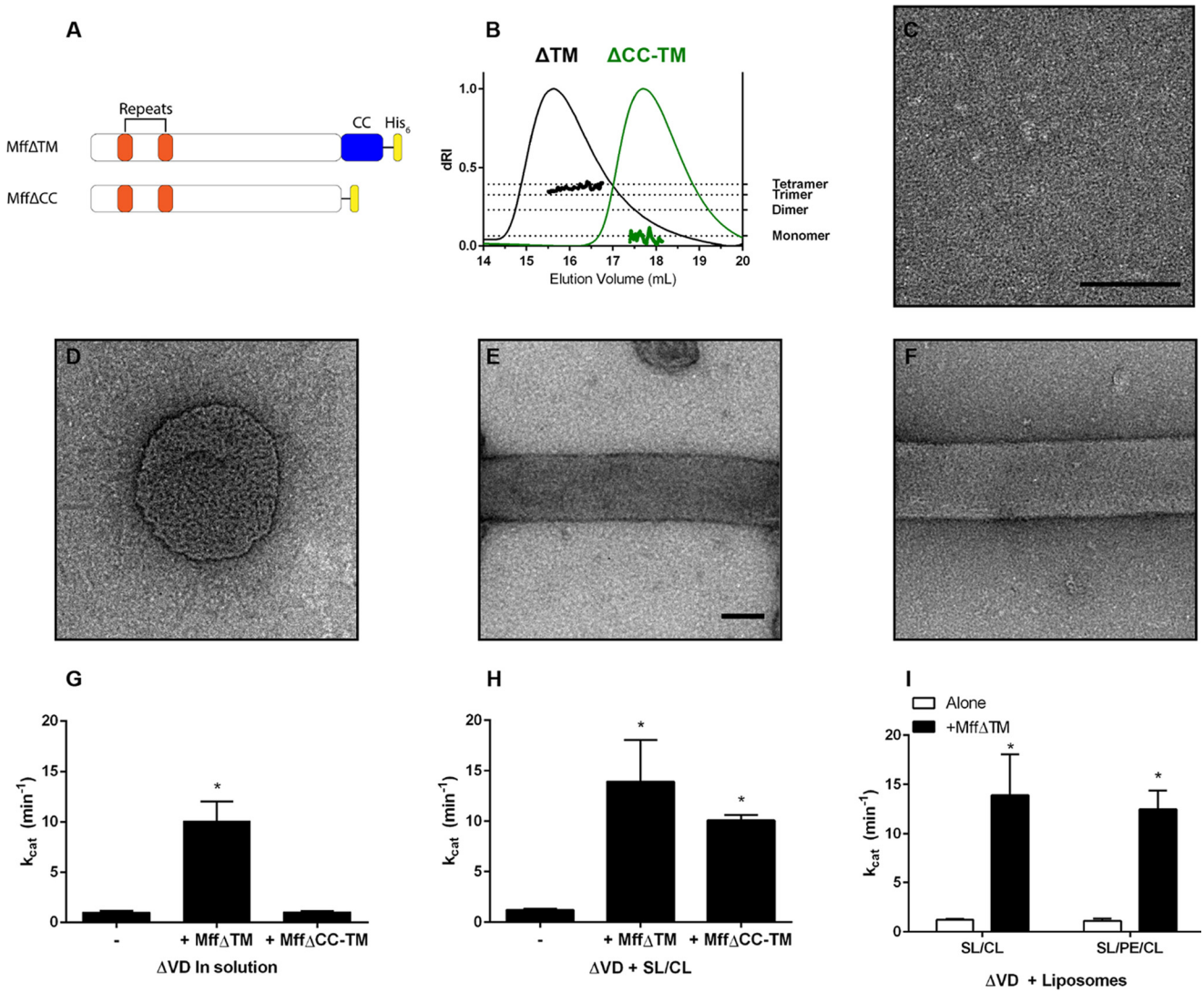

FIGURE 6. **Oligomerization of Mff cytosolic domains promotes Mff-induced Drp1 self-assembly.** *A*, schematic representation of the Mff constructs used in this study, including MffΔTM and MffΔCC-TM. The N-terminal repeat segments (*orange*), CC motif (*blue*), and C-terminal His_6 tag (*yellow*) are highlighted. *B*, SEC-MALS was used to determine the multimeric state of MffΔTM (*black*) and MffΔCC-TM (*green*). *Dotted lines* indicate the predicted molecular masses of Mff multimers. *dRI*, normalized differential refractive index. *C–F*, negative stain EM images of ΔVD in the presence of MffΔCC-TM in solution (*C*), in the presence of undecorated liposomes containing PE (25%) and CL (10%) (SL/PE/CL) (*D*), in the presence of MffΔTM tethered to the same liposomes (SL/PE/CL/MffΔTM) (*E*), or in the presence of MffΔCC-TM tethered to liposomes lacking PE (SL/CL) (*F*). *Scale bars*, 100 nm. *G–H*, GTPase activity of ΔVD was measured alone and in the presence of MffΔTM or MffΔCC-TM in solution (*G*) or tethered to SL/CL (*H*). *I*, ΔVD activity was also measured in the absence (*white*) or presence (*black*) of MffΔTM coupled to SL/CL and SL/PE/CL lipid templates as indicated. *, $p < 0.0005$.

containing 35 mol % PE. When ΔVD was added alone, no interaction was observed with the SL/PE/CL template (Fig. 6*D*). However, when the same template was decorated with MffΔTM, the addition of ΔVD led to the formation of well ordered protein-lipid tubules (Fig. 6*E*). Interestingly, the Mff-induced stimulation in GTPase activity was not enhanced by the helical polymerization of ΔVD. Rather, Mff decoration of SL/CL or SL/PE/CL templates yielded comparable increases in activity (Fig. 6*I*) despite the apparent differences in structure (disconnected filaments *versus* a tightly packed helical lattice; Figs. 5*C* and 6*F*, respectively). Nevertheless, incorporation of PE enhanced the fluidity of the lipid template and allowed the Mff tetramer complex to recruit Drp1 polymers that deformed the membrane. This demonstrates the ability of Mff to nucleate Drp1 polymerization at sites of active membrane remodeling.

Discussion

Genetic and cellular studies have clearly demonstrated the importance of Mff in recruiting Drp1 to the OMM (29, 30). However, it remained unclear how Mff directly influences Drp1 function and cellular localization. These studies reveal the inherent ability of Mff to stimulate Drp1 self-assembly and GTPase activity *in vitro*. Previously, this role remained uncharacterized because Drp1-Mff interactions are transient and strongly influenced by the oligomeric tendencies of both proteins. Factors that alter the assembly properties of either, or both, proteins have the potential to alter interactions within this mitochondrial fission complex.

Initially, the role of the VD was examined based on its apparent proximity to the membrane as well as its ability to interact with CL (21, 23, 25). This proposed location would also place it

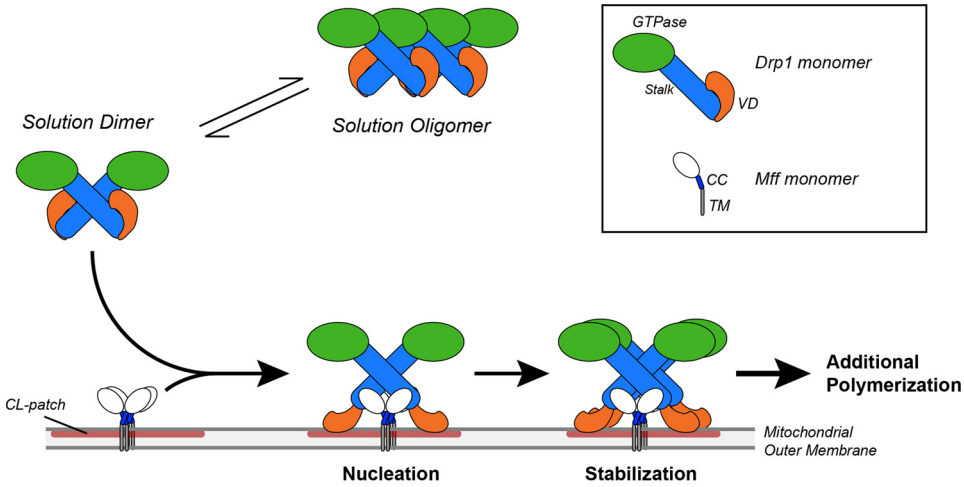

FIGURE 7. **Mff selectively promotes oligomerization of assembly-competent Drp1 dimers.** WT Drp1 exists as a mixture of multimeric species in solution (dimers and larger multimers, *black arrows*). Coincident interaction of the VD with CL in the membrane (*red area* of the bilayer) relieves its regulatory effect, which stabilizes Drp1 dimer interactions with Mff to promote assembly of the fission machinery.

directly adjacent to receptor proteins on the OMM to promote intermolecular interactions. Despite this proximity to partner proteins at the surface of the membrane, our results show that the VD indirectly regulates Drp1 interactions with partner proteins by modulating its oligomeric propensity. Interestingly, Mff selectively assembles dimeric Drp1, which represents a subset of Drp1 multimers observed in these studies. Because the ΔVD mutant yields exclusively dimeric species, an enhanced cooperative interaction with Mff was observed. Self-assembly of the ΔVD dimers in the presence of Mff led to formation of filaments with a diameter of ~24 nm. This parallels the ~23-nm width of Drp1 polymers observed in the crystal lattice used to determine the atomic structure of Drp1 (22). This geometry suggests that the Drp1 middle domain and GED interfaces are responsible for the formation of these filamentous structures.

Correspondingly, when Drp1 self-assembly is disrupted by the G363D mutation, Mff-induced self-assembly and stimulated activity is ablated. Thus, Mff guides productive Drp1 self-assembly, and augmentation of Drp1 activity is not due to Mff interactions alone. Instead, maximal stimulation of ΔVD GTPase activity was achieved upon formation of extended filamentous structures in the presence of Mff in solution and at the membrane. Therefore, the fundamental mechanism of Drp1 activation by Mff is independent of lipid interactions, and is instead a direct result of intermolecular contacts that are enhanced with the ΔVD mutant. This indicates that Mff coordinates Drp1 self-assembly, which enhances its activity.

Unlike ΔVD, WT Drp1 interactions with Mff are regulated by the diversity of multimers formed in solution. Drp1 interchanges among dimers and higher-order multimers at physiologic salt concentrations (23), and we propose that larger oligomers are unable to form functional interactions with Mff. While this manuscript was in revision, another study implied that Mff selectively recruits oligomeric Drp1 (35); however, our results are clearly incongruent with this finding. In point of fact, the R376E mutation within Drp1 alters its assembly properties and favors higher-order multimers in solution that impede functional interactions with Mff. Interestingly, this change is dependent on the VD as deletion of this region rescues the dimeric tendencies of the R376E mutant, and functional interactions with Mff are restored. Therefore, this residue directly influences the conformational sampling of the VD and its ability to regulate Drp1 oligomerization.

Correspondingly, VD interactions with the membrane can influence cooperative Drp1-Mff interactions. We determined that when full-length Drp1-3 was incubated with Mff tethered-liposomes containing limited amounts of CL, the stimulation in activity was greater than when Mff was coupled to liposomes lacking CL. Moreover, this effect was abolished when the VD was removed. Thus, interactions between the VD and the membrane have the potential to stabilize Drp1 dimers and promote cooperative interactions with Mff. In fact, the accompanying article (42) clearly shows that Mff stimulation of Drp1 activity is synergistic with CL stimulation. These results are congruent with previous reports of VD interactions with CL that promote Drp1 recruitment to lipid bilayers (21, 23–25). Given that CL has been shown to stabilize dimeric Drp1 at the lipid surface to promote Drp1 self-assembly (23), we propose that CL interactions at the membrane directly promote Drp1 dimer interactions with Mff (Fig. 7).

Interestingly, the same stimulation was not seen when Drp1-1 was added to Mff-decorated liposomes. Therefore, the presence of the 37-amino acid B-insert within the VD can further regulate Drp1 interactions with Mff as shown in the accompanying article (42). Given that as many as eight isoforms of Drp1 (34, 41) and at least nine splice variants of Mff have been identified (30), the potential complexity of interactions that are regulated by sequence changes is vast. Regardless, these results demonstrate how natural sequence modifications alter interactions between Drp1 and one of its receptors. Native sequence changes in this region due to alternative splicing and post-translational modifications have the potential to "tune" Drp1 interactions with partner proteins by altering its assembly properties.

In line with previous studies (22, 40), we also confirmed that disruption of the variable domain sequence altered the effi-

ciency of mitochondrial fission in cells. Although we clearly demonstrate that ΔVD is hypomorphic when compared with WT when expressed in cells lacking Drp1, significant mitochondrial fission activity is retained. We also show that ΔVD is recruited to mitochondria in a predominantly Mff-dependent manner. Previous studies have differed in their assessments of ΔVD function, as removal of this region has been proposed to both enhance and impair mitochondrial fission. This discrepancy may be due to the design of the VD deletion constructs, the level of overexpression, and the cell lines used in these studies. We find clear mitochondrial localization in our analyses, which indicates that the hypomorphic phenotype is likely due to post-recruitment activity. This agrees with recent experiments showing that ΔVD can tubulate liposomes *in vitro*, but GTP-induced constriction of these membranes is diminished when compared with WT Drp1 (14). Consequently, ΔVD-induced constriction may result in infrequent membrane scission, consistent with the observed decrease in mitochondrial fragmentation. Taken together with our biochemical observations, these results reveal that the fundamental role of Mff is to provide a scaffold for Drp1 self-assembly, and molecular alterations that change the assembly properties of Drp1 or Mff can regulate this interaction.

The present lack of structural information for Mff makes it hard to predict where direct interaction sites would reside, and structural prediction software suggests that the cytosolic portion of Mff is largely disordered. One exception is the CC motif, which is predicted to form a helical segment adjacent to the C-terminal TM region, which promotes Mff self-assembly. Consistent with this prediction, Mff was found to exist as a stable tetramer in solution, which enhances the ability of Mff to coordinate Drp1 interactions as evidenced by the formation of Drp1 filaments in solution and proximal to membrane templates. Removal of the CC resulted in Mff monomers that could not stabilize Drp1 interactions in solution. Still, the use of a lipid template enhanced the local concentration of MffΔCC-TM and provided an adequate scaffold for Drp1 recruitment and self-assembly. Moreover, membrane tubulation was observed, which suggests that flexibility within the scaffold and/or lipid template determines the extent to which Drp1 can impart curvature on the membrane. Accordingly, incorporation of PE to the more rigid SL/CL template enhanced membrane fluidity and/or lateral movement of the Mff tetramer such that Drp1 oligomerization was able to deform the membrane and generate tubular structures. Based on these results, Mff provides a platform for the nucleation of Drp1 oligomers that subsequently impose curvature on the underlying membrane.

Overall, we propose a model wherein Drp1 dimers selectively interact with cytosolic segments of Mff tetramers (Fig. 7) to constitute functional copolymers, and mutations or factors that alter the oligomeric state of Drp1 affect the efficiency of its recruitment to the OMM. In addition, membrane interactions have the potential to stabilize Drp1-Mff complexes localized at mitochondrial constriction sites. Moving forward, the versatile tools employed in this study provide a means to explore how Drp1 interactions with different adaptor proteins on the OMM regulate its structure and activity.

Author Contributions—R. W. C. conceived, coordinated, and performed the experiments for this study and wrote the paper. C. A. F. prepared the vectors for expression of the natural Drp1 splice variants. R. R. performed and provided technical expertise for the SEC-MALS experiments and subsequent data analyses. X. Q. performed and provided technical expertise and analysis for all experiments with cultured MEF cells. J. A. M. assisted in the design and analysis of the experiments in this study, and with the preparation of the paper. All authors have reviewed the results and approved the final version of the manuscript.

Acknowledgments—We thank Heather Holdaway and Hisashi Fujioka for their expertise and advice with electron microscopy studies. We acknowledge Hiromi Sesaki and David Chan for providing Drp1 and Mff knock-out MEFs, respectively.

References

1. Berman, S. B., Pineda, F. J., and Hardwick, J. M. (2008) Mitochondrial fission and fusion dynamics: the long and short of it. *Cell Death Differ.* **15,** 1147–1152
2. Chan, D. C. (2006) Mitochondrial fusion and fission in mammals. *Annu. Rev. Cell Dev. Biol.* **22,** 79–99
3. Chen, H., and Chan, D. C. (2009) Mitochondrial dynamics–fusion, fission, movement, and mitophagy—in neurodegenerative diseases. *Hum. Mol. Genet* **18,** R169—R176
4. Knott, A. B., Perkins, G., Schwarzenbacher, R., and Bossy-Wetzel, E. (2008) Mitochondrial fragmentation in neurodegeneration. *Nat. Rev. Neurosci.* **9,** 505–518
5. Ashrafian, H., Docherty, L., Leo, V., Towlson, C., Neilan, M., Steeples, V., Lygate, C. A., Hough, T., Townsend, S., Williams, D., Wells, S., Norris, D., Glyn-Jones, S., Land, J., Barbaric, I., Lalanne, Z., Denny, P., Szumska, D., Bhattacharya, S., Griffin, J. L., Hargreaves, I., Fernandez-Fuentes, N., Cheeseman, M., Watkins, H., and Dear, T. N. (2010) A mutation in the mitochondrial fission gene *Dnm1l* leads to cardiomyopathy. *PLoS Genet.* **6,** e1001000
6. Ong, S. B., and Hausenloy, D. J. (2010) Mitochondrial morphology and cardiovascular disease. *Cardiovasc. Res.* **88,** 16–29
7. Ju, W. K., Liu, Q., Kim, K. Y., Crowston, J. G., Lindsey, J. D., Agarwal, N., Ellisman, M. H., Perkins, G. A., and Weinreb, R. N. (2007) Elevated hydrostatic pressure triggers mitochondrial fission and decreases cellular ATP in differentiated RGC-5 cells. *Invest. Ophthalmol. Vis. Sci.* **48,** 2145–2151
8. Cassidy-Stone, A., Chipuk, J. E., Ingerman, E., Song, C., Yoo, C., Kuwana, T., Kurth, M. J., Shaw, J. T., Hinshaw, J. E., Green, D. R., and Nunnari, J. (2008) Chemical inhibition of the mitochondrial division dynamin reveals its role in Bax/Bak-dependent mitochondrial outer membrane permeabilization. *Dev. Cell* **14,** 193–204
9. Guo, X., Disatnik, M. H., Monbureau, M., Shamloo, M., Mochly-Rosen, D., and Qi, X. (2013) Inhibition of mitochondrial fragmentation diminishes Huntington's disease-associated neurodegeneration. *J. Clin. Invest.* **123,** 5371–5388
10. Lackner, L. L., and Nunnari, J. (2010) Small molecule inhibitors of mitochondrial division: tools that translate basic biological research into medicine. *Chem. Biol.* **17,** 578–583
11. Ong, S. B., Subrayan, S., Lim, S. Y., Yellon, D. M., Davidson, S. M., and Hausenloy, D. J. (2010) Inhibiting mitochondrial fission protects the heart against ischemia/reperfusion injury. *Circulation* **121,** 2012–2022
12. Park, S. W., Kim, K. Y., Lindsey, J. D., Dai, Y., Heo, H., Nguyen, D. H., Ellisman, M. H., Weinreb, R. N., and Ju, W. K. (2011) A selective inhibitor of Drp1, Mdivi-1, increases retinal ganglion cell survival in acute ischemic mouse retina. *Invest. Ophthalmol. Vis. Sci.* **52,** 2837–2843
13. Su, Y. C., and Qi, X. (2013) Inhibition of excessive mitochondrial fission reduced aberrant autophagy and neuronal damage caused by LRRK2 G2019S mutation. *Hum. Mol. Genet* **22,** 4545–4561
14. Francy, C. A., Alvarez, F. J., Zhou, L., Ramachandran, R., and Mears, J. A. (2015) The mechanoenzymatic core of dynamin-related protein 1 com-

prises the minimal machinery required for membrane constriction. *J. Biol. Chem.* **290,** 11692–11703
15. Mears, J. A., Lackner, L. L., Fang, S., Ingerman, E., Nunnari, J., and Hinshaw, J. E. (2011) Conformational changes in Dnm1 support a contractile mechanism for mitochondrial fission. *Nat. Struct. Mol. Biol.* **18,** 20–26
16. Qi, X., Qvit, N., Su, Y. C., and Mochly-Rosen, D. (2013) A novel Drp1 inhibitor diminishes aberrant mitochondrial fission and neurotoxicity. *J. Cell Sci.* **126,** 789–802
17. Smirnova, E., Shurland, D. L., Ryazantsev, S. N., and van der Bliek, A. M. (1998) A human dynamin-related protein controls the distribution of mitochondria. *J. Cell Biol.* **143,** 351–358
18. Chang, C. R., Manlandro, C. M., Arnoult, D., Stadler, J., Posey, A. E., Hill, R. B., and Blackstone, C. (2010) A lethal *de novo* mutation in the middle domain of the dynamin-related GTPase Drp1 impairs higher order assembly and mitochondrial division. *J. Biol. Chem.* **285,** 32494–32503
19. Zhu, P. P., Patterson, A., Stadler, J., Seeburg, D. P., Sheng, M., and Blackstone, C. (2004) Intra- and intermolecular domain interactions of the C-terminal GTPase effector domain of the multimeric dynamin-like GTPase Drp1. *J. Biol. Chem.* **279,** 35967–35974
20. Yoon, Y., Pitts, K. R., and McNiven, M. A. (2001) Mammalian dynamin-like protein DLP1 tubulates membranes. *Mol. Biol. Cell* **12,** 2894–2905
21. Bustillo-Zabalbeitia, I., Montessuit, S., Raemy, E., Basañez, G., Terrones, O., and Martinou, J. C. (2014) Specific interaction with cardiolipin triggers functional activation of dynamin-related protein 1. *PLoS ONE* **9,** e102738
22. Fröhlich, C., Grabiger, S., Schwefel, D., Faelber, K., Rosenbaum, E., Mears, J., Rocks, O., and Daumke, O. (2013) Structural insights into oligomerization and mitochondrial remodelling of dynamin 1-like protein. *EMBO J.* **32,** 1280–1292
23. Macdonald, P. J., Stepanyants, N., Mehrotra, N., Mears, J. A., Qi, X., Sesaki, H., and Ramachandran, R. (2014) A dimeric equilibrium intermediate nucleates Drp1 reassembly on mitochondrial membranes for fission. *Mol. Biol. Cell* **25,** 1905–1915
24. Stepanyants, N., Macdonald, P. J., Francy, C. A., Mears, J. A., Qi, X., and Ramachandran, R. (2015) Cardiolipin's propensity for phase transition and its reorganization by dynamin-related protein 1 form a basis for mitochondrial membrane fission. *Mol. Biol. Cell* **26,** 3104–3116
25. Ugarte-Uribe, B., Müller, H. M., Otsuki, M., Nickel, W., and García-Sáez, A. J. (2014) Dynamin-related protein 1 (Drp1) promotes structural intermediates of membrane division. *J. Biol. Chem.* **289,** 30645–30656
26. Bui, H. T., and Shaw, J. M. (2013) Dynamin assembly strategies and adaptor proteins in mitochondrial fission. *Curr. Biol.* **23,** R891–R899
27. Elgass, K., Pakay, J., Ryan, M. T., and Palmer, C. S. (2013) Recent advances into the understanding of mitochondrial fission. *Biochim. Biophys. Acta* **1833,** 150–161
28. Losón, O. C., Song, Z., Chen, H., and Chan, D. C. (2013) Fis1, Mff, MiD49, and MiD51 mediate Drp1 recruitment in mitochondrial fission. *Mol. Biol. Cell* **24,** 659–667
29. Otera, H., Wang, C., Cleland, M. M., Setoguchi, K., Yokota, S., Youle, R. J., and Mihara, K. (2010) Mff is an essential factor for mitochondrial recruitment of Drp1 during mitochondrial fission in mammalian cells. *J. Cell Biol.* **191,** 1141–1158
30. Gandre-Babbe, S., and van der Bliek, A. M. (2008) The novel tail-anchored membrane protein Mff controls mitochondrial and peroxisomal fission in mammalian cells. *Mol. Biol. Cell* **19,** 2402–2412
31. Koirala, S., Guo, Q., Kalia, R., Bui, H. T., Eckert, D. M., Frost, A., and Shaw, J. M. (2013) Interchangeable adaptors regulate mitochondrial dynamin assembly for membrane scission. *Proc. Natl. Acad. Sci. U.S.A.* **110,** E1342–E1351
32. Otera, H., and Mihara, K. (2011) Discovery of the membrane receptor for mitochondrial fission GTPase Drp1. *Small GTPases* **2,** 167–172
33. Leonard, M., Song, B. D., Ramachandran, R., and Schmid, S. L. (2005) Robust colorimetric assays for dynamin's basal and stimulated GTPase activities. *Methods Enzymol.* **404,** 490–503
34. Strack, S., Wilson, T. J., and Cribbs, J. T. (2013) Cyclin-dependent kinases regulate splice-specific targeting of dynamin-related protein 1 to microtubules. *J. Cell Biol.* **201,** 1037–1051
35. Liu, R., and Chan, D. C. (2015) The mitochondrial fission receptor Mff selectively recruits oligomerized Drp1. *Mol. Biol. Cell* **26,** 4466–4477
36. Esposito, E. A., Shrout, A. L., and Weis, R. M. (2008) Template-directed self-assembly enhances RTK catalytic domain function. *J. Biomol. Screen* **13,** 810–816
37. Shrout, A. L., Esposito, E. A., 3rd, and Weis, R. M. (2008) Template-directed assembly of signaling proteins: a novel drug screening and research tool. *Chem. Biol. Drug. Des.* **71,** 278–281
38. Wakabayashi, J., Zhang, Z., Wakabayashi, N., Tamura, Y., Fukaya, M., Kensler, T. W., Iijima, M., and Sesaki, H. (2009) The dynamin-related GTPase Drp1 is required for embryonic and brain development in mice. *J. Cell Biol.* **186,** 805–816
39. Tanaka, A., Kobayashi, S., and Fujiki, Y. (2006) Peroxisome division is impaired in a CHO cell mutant with an inactivating point-mutation in dynamin-like protein 1 gene. *Exp. Cell Res.* **312,** 1671–1684
40. Strack, S., and Cribbs, J. T. (2012) Allosteric modulation of Drp1 mechanoenzyme assembly and mitochondrial fission by the variable domain. *J. Biol. Chem.* **287,** 10990–11001
41. Chen, C. H., Howng, S. L., Hwang, S. L., Chou, C. K., Liao, C. H., and Hong, Y. R. (2000) Differential expression of four human dynamin-like protein variants in brain tumors. *DNA Cell Biol.* **19,** 189–194
42. Macdonald, P. J., Francy, C. A., Stepanyants, N., Lehman, L.,Baglio, A., Mears, J. A., Qi, X., Ramachandran, R. (2015) Distinct splice variants of dynamin-related protein 1 differentially utilize mitochondrial fission factor as an effector of cooperative GTPase activity. *J. Biol. Chem.* **291,** 493–507